

Power-factor control of the LCC current-output resonant converter

A. J. Gilbert, C. M. Bingham*, D. A. Stone, M. P. Foster

SHEFFIELD UNIVERSITY

Department of Electronic & Electrical Engineering
Mappin Street, Sheffield, S1 3JD, U.K.

Tel.: +44/ (0)114 222 5355

*E-Mail: c.m.bingham@sheffield.ac.uk

URL: <http://www.sheffield.ac.uk/eee>

Keywords

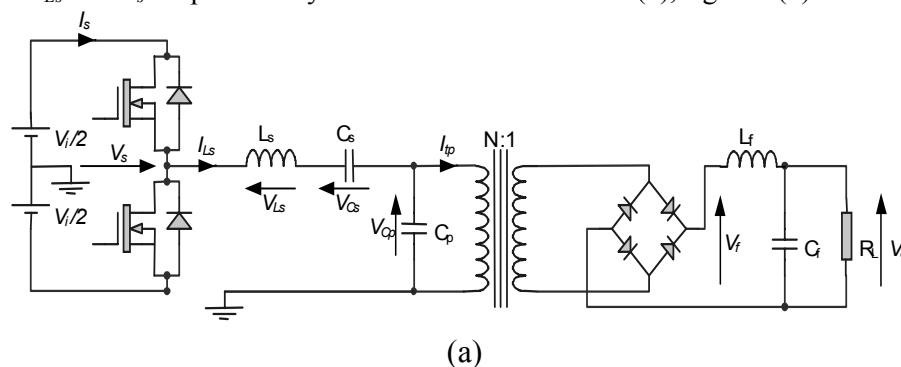
Resonant converter, Converter control, ZVS converters, DC power supply, High frequency power converter

Abstract

An improved control strategy for LCC current-output resonant converters is proposed. Small/large-signal converter models and the steady-state dynamics of the converter are used for controlling power-factor. The proposed method provides a convenient, linear control mechanism for the design of regulators, which has a similar influence to varying the DC-link supply voltage in terms of output-voltage/current control, which, whilst being desirable, is normally not a realistic proposition for commercial supplies.

Introduction

It is well established that resonant converters are advantageous in-terms of size and efficiency [1,2]. Currently one of the main drawbacks for the use of resonant converters, however, is the lack of literature on robust control of such systems. Here, a novel control strategy is therefore considered, that approximately linearises the behaviour of the converter such that traditional control techniques can be applied. The technique is applied to the LCC current-output resonant converter as shown in Figure 1(a). Although other control strategies [3,4] aim to linearise the converter behaviour, none linearise the behaviour as fully as presented here. Hardware implementation is via integration of V_{Ls} using a very low pass filter (RC network) to give precise zero-crossings of I_{Ls} , and a real-time FPGA based delay network that controls the MOSFET switching times such that based on the previous cycle, the phase angle between I_{Ls} and V_s is specified by the controllers desired $\cos(\theta)$, figure 1(b).



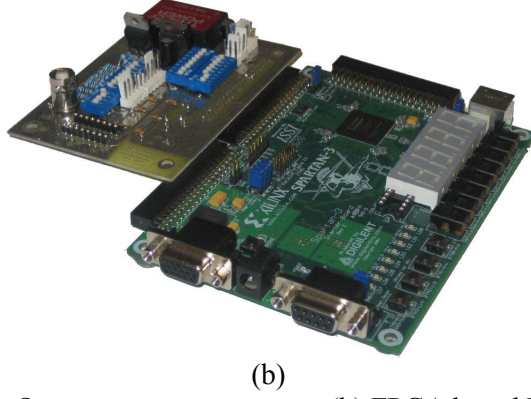


Fig. 1: (a)LCC Current-Output resonant converter (b) FPGA based Power-factor controller

Equivalence of power-factor and supply voltage control

During normal operation, the resonant tank is excited above the resonant frequency by an applied square-wave switching voltage, V_s , that results in an approximately sinusoidal series inductor current I_{Ls} , see Fig. 2(a). The fundamental component of the square-wave is also shown in Fig.2, and can be sub-divided into two sinusoidal components, one in phase with the resonant current, I_{Ls} , and one in quadrature, Fig.2(b).

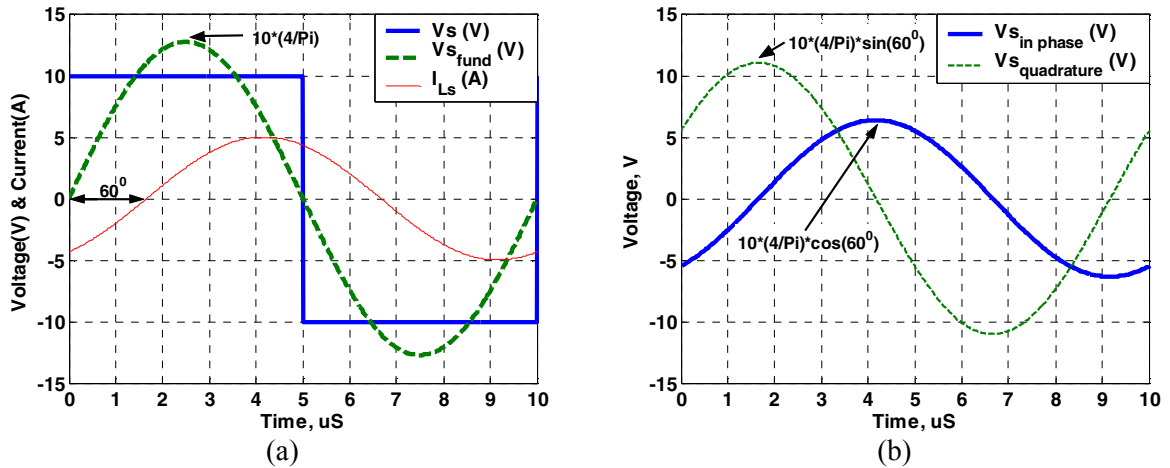


Fig. 2: (a) Switching voltage and resonant tank current
(b) phase components of switching voltage wrt. resonant tank current.

The following identity will be used to derive the magnitude of the switching voltage component in phase with the series inductor current.

$$\sin(A+B) = \sin(A)\cos(B) + \cos(A)\sin(B) \quad (1)$$

The switching voltage can be approximated by its fundamental component as follows:

$$V_s = \frac{V_{dc}}{2} \text{sgn}(\sin(\omega_s t)) \approx \frac{2V_{dc}}{\pi} \sin(\omega_s t) \quad (2)$$

The series inductor current can be approximated by a sinusoid as follows:

$$I_{Ls} = \hat{I}_{Ls} \sin(\omega_s t - \theta) \quad (3)$$

Using the identity in (1) the fundamental component is equated to a sinusoid in-phase with the series inductor current and another in quadrature:

$$\frac{2V_{dc}}{\pi} \sin(\omega_s t) = \frac{2V_{dc}}{\pi} \cos(\theta) \sin(\omega_s t - \theta) + \frac{2V_{dc}}{\pi} \sin(\theta) \cos(\omega_s t - \theta) \quad (4)$$

To maintain the real power flow into the converter, assuming a square-wave switching voltage in phase with the series inductor current, the ‘equivalent’ square-wave would take the form:

$$V_s = \frac{V_{dc}}{2} \cos(\theta) \text{sgn}(\sin(\omega_s t - \theta)) = \frac{V_{dc} PF}{2} \text{sgn}(\sin(\omega_s t - \theta)) \quad \text{where } PF = \cos(\theta) \quad (5)$$

Varying the instantaneous power-factor (PF) is therefore equivalent to varying the instantaneous supply-voltage, from a fundamental mode approximation (FMA) perspective, i.e the current waveform is assumed sinusoidal. When deriving a small-signal model of the converter, this allows the converter to be considered as switching at the resonant frequency whilst varying the power factor—the power-factor is included in the model as a supply-voltage scaling factor. Note that, from this perspective, the power-factor bias will not change the small-signal model.

By way of example, Fig.3 compares the experimentally measured small-signal frequency response with that predicted by the proposed analysis. Experimentally the power factor is perturbed for the following converter: $V_{dc}=18$, $L_s=13.6\mu\text{H}$, $C_s=220\text{nF}$, $C_p=130\text{nF}$, $N=1$, $L_f=24\mu\text{H}$, $C_f=220\mu\text{F}$, around $PF_{bias}=0.75$ through use of a self-oscillating power-factor controller.

When $R_L=10\Omega$, the converter gain at resonance is 0.674 hence with the specified input voltage, $V_{out}=12.1\text{V}$. This implies a steady-state gain of +21.7dB at 0Hz between power-factor and output-voltage.

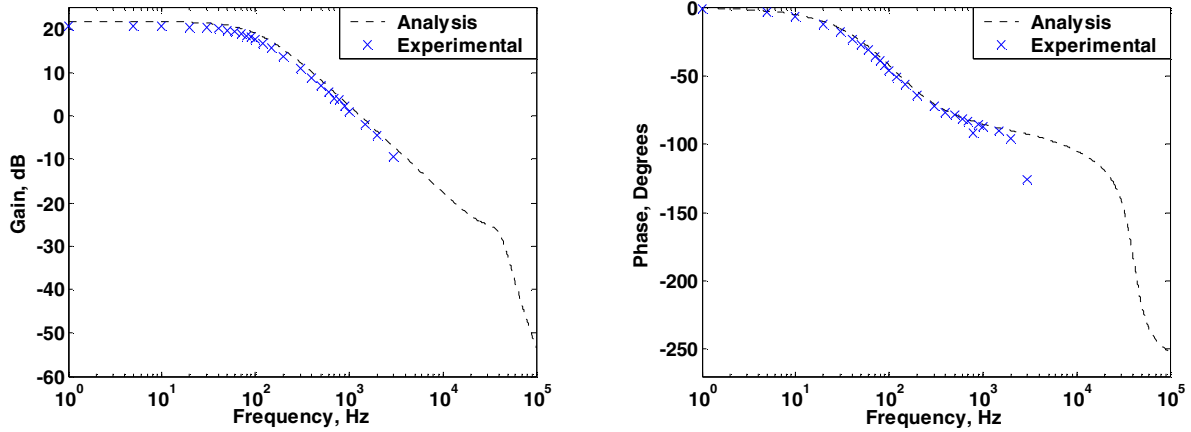


Fig 3: Small-signal frequency response comparison between proposed analysis and experimental results for 10Ω load. Note that above a 2kHz perturbation in power factor, the phase response measurements become inaccurate as a result of the signal-level becoming comparable in amplitude with noise and output-voltage ripple.

A high degree of correlation is present, thereby confirming that the proposed analysis is indeed valid.

Phasor-transform converter model at the resonant frequency

To enable a small-signal model of the power-factor controlled converter to be derived, a large-signal phasor-transformed model is first generated for the converter operating at the resonant frequency.

Traditionally, the d-q-0 axis transformation is used for the modelling and analysis of 3-phase machines and power systems. However, there also exists a similar phasor-transform technique for single-phase systems based on the assumption that the signals are sinusoidal in nature but vary in amplitude, frequency and phase [5,6]. These features are characteristic of resonant converters operating near resonance with sufficiently high quality factor—as commonly encountered. The presented analysis is based on the LCC current-output converter, Figure 1.

A sinusoidal voltage or current can be approximated by a sinusoid whose frequency and amplitude vary with time [5]:

$$x(t) = \Re \left(\bar{x}(t) e^{j \int \omega_s(t) dt} \right) \quad (6)$$

where $\bar{x}(t)$ is the complex envelope of $x(t)$ and ω_s is the switching frequency. Initially, consider the differential equation governing the behaviour of an ideal inductor:

$$v(t) = L \frac{d i(t)}{dt} \quad (7)$$

Substituting (6) into (7) for current and voltage gives:

$$\Re \left(\bar{v}(t) e^{j \int \omega_s(t) dt} \right) = L \frac{d}{dt} \Re \left(\bar{i}(t) e^{j \int \omega_s(t) dt} \right) \quad (8)$$

and simplifying gives [7]:

$$\bar{v}(t) = L \frac{d \bar{i}(t)}{dt} + j L \omega_s(t) \bar{i}(t) \quad (9)$$

In a similar manner, capacitors and resistors are described by:

$$\bar{i}(t) = C \frac{d \bar{v}(t)}{dt} + j C \omega_s(t) \bar{v}(t) \quad (10a)$$

$$\bar{v}(t) = R \bar{i}(t) \quad (10b)$$

More generally, therefore, a signal envelope $\bar{x}(t)$ can be expanded into its constituent real and imaginary components, denoted by 'r' and 'i' subscripts, respectively.

$$\bar{x}(t) = x_r(t) + j x_i(t) \quad (11)$$

For the inductor, substituting (11) into (9) and separating the real and imaginary components gives:

$$v_r(t) = L \frac{d i_r(t)}{dt} - L \omega_s(t) i_i(t) \quad (12a)$$

$$v_i(t) = L \frac{d i_i(t)}{dt} + L \omega_s(t) i_r(t) \quad (12b)$$

and for the capacitor and resistor,

$$i_r(t) = C \frac{d v_r(t)}{dt} - C \omega_s(t) v_i(t) \quad (13a)$$

$$i_i(t) = C \frac{d v_i(t)}{dt} + C \omega_s(t) v_r(t) \quad (13b)$$

$$v_r(t) = R i_r(t) \quad (14a)$$

$$v_i(t) = R i_i(t) \quad (14b)$$

For use in network simulators such as SPICE, for instance, the complex components can be eliminated through use of two coupled equivalent circuits, one describing the real domain and the other the imaginary domain [8].

The rectifier in Fig. 1 is not readily modelled using the phasor-transform, and requires the resonant tank and output filter to be modelled separately, and then combined. This is justified since the output filter bandwidth is much lower than that of the resonant tank, and, as a result of the rectifier action, the filter effectively reacts only to the envelope of the resonant tank waveforms. From basic Fundamental Mode Approximation (FMA), the resonant tank is modelled as in Fig.4—see [2].

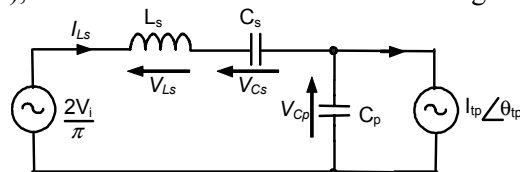


Fig 4: FMA model of LCC Resonant tank

After phasor-transforming the components in Fig. 4, the coupled networks shown in Fig. 5 are obtained.

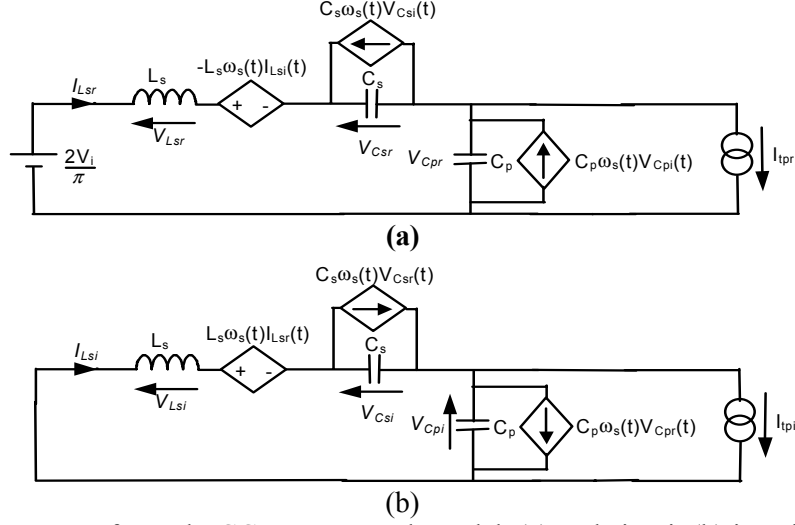


Fig. 5 : Phasor transformed LCC resonant tank model (a) real circuit (b) imaginary circuit
A state space representation of Fig. 5 is obtained for both the real and imaginary circuits, which are then combined to give:

$$\begin{bmatrix} \dot{I}_{Lsr} \\ V_{Cs_r} \\ V_{Cp_r} \\ I_{Lsi} \\ V_{Cs_i} \\ V_{Cp_i} \end{bmatrix} = \begin{bmatrix} 0 & -\frac{1}{L_s} & -\frac{1}{L_s} & \omega_s & 0 & 0 \\ \frac{1}{C_s} & 0 & 0 & 0 & \omega_s & 0 \\ \frac{1}{C_p} & 0 & 0 & 0 & 0 & \omega_s \\ -\omega_s & 0 & 0 & 0 & -\frac{1}{L_s} & -\frac{1}{L_s} \\ 0 & -\omega_s & 0 & \frac{1}{C_s} & 0 & 0 \\ 0 & 0 & -\omega_s & \frac{1}{C_p} & 0 & 0 \end{bmatrix} \begin{bmatrix} I_{Lsr} \\ V_{Cs_r} \\ V_{Cp_r} \\ I_{Lsi} \\ V_{Cs_i} \\ V_{Cp_i} \end{bmatrix} + \begin{bmatrix} \frac{2}{\pi L_s} & 0 & 0 \\ 0 & 0 & 0 \\ 0 & -\frac{1}{C_p} & 0 \\ 0 & 0 & 0 \\ 0 & 0 & 0 \\ 0 & 0 & -\frac{1}{C_p} \end{bmatrix} \begin{bmatrix} V_i \\ I_{pr} \\ I_{pi} \end{bmatrix} \quad (15)$$

The waveform envelopes are extracted using the output equation:

$$\begin{bmatrix} \hat{I}_{Lsr} \\ \hat{V}_{Cs_r} \\ \hat{V}_{Cp_r} \\ \hat{I}_{Lsi} \\ \hat{V}_{Cs_i} \\ \hat{V}_{Cp_i} \end{bmatrix} \equiv \begin{bmatrix} 1 & 0 & 0 & j & 0 & 0 \\ 0 & 1 & 0 & 0 & j & 0 \\ 0 & 0 & 1 & 0 & 0 & j \end{bmatrix} \begin{bmatrix} I_{Lsr} \\ V_{Cs_r} \\ V_{Cp_r} \\ I_{Lsi} \\ V_{Cs_i} \\ V_{Cp_i} \end{bmatrix} \quad (16)$$

Finally, the output filter is described in state-variable form by:

$$\begin{bmatrix} \dot{I}_{Lf} \\ \dot{V}_o \end{bmatrix} = \begin{bmatrix} 0 & -\frac{1}{L_f} \\ \frac{1}{C_f} & -\frac{1}{R_L C_f} \end{bmatrix} \begin{bmatrix} I_{Lf} \\ V_o \end{bmatrix} + \begin{bmatrix} 1 \\ 0 \end{bmatrix} \frac{1}{L_f} [V_f] \quad (17)$$

The voltages of the phasor-transformed tank model and output filter are coupled by noting that the average voltage presented to the output filter, via the rectifier, is given by (18) since V_{Cp} is assumed sinusoidal.

$$V_f = \frac{2 \hat{V}_{Cp}}{N\pi} \quad (18)$$

Coupling of the currents is achieved by replacing the current source in Fig. 4 by a time varying resistor, Fig. 6, with the imaginary and real components of I_{tp} given by:

$$I_{tp_r} = \frac{V_{Cp_r}}{R_{filt}} \quad (19a)$$

$$I_{tp_i} = \frac{V_{Cp_i}}{R_{filt}} \quad (19b)$$

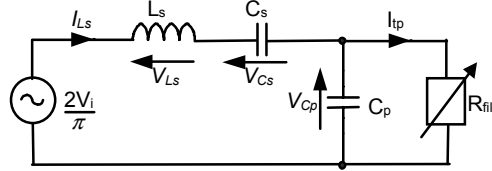


Fig. 6: Modelling output filter by a time varying load

Since the transformer primary current is a squarewave, and the fundamental is used in the phasor-transformed model, the peak of the squarewave current is scaled by $4/\pi$.

$$\hat{I}_{tp} = \sqrt{I_{tp_r}^2 + I_{tp_i}^2} = \frac{4I_{Lf}}{N\pi} \quad (20)$$

The time-varying load resistance is now calculated from:

$$R_{filt} = \frac{\hat{V}_{Cp}}{\hat{I}_{tp}} \quad (21)$$

From (19),(20) and (21) the transformer primary phasor currents are found algebraically:

$$I_{tp_r} = \frac{4I_{Lf}}{N\pi} \frac{V_{Cp_r}}{\hat{V}_{Cp}} \quad (22a)$$

$$I_{tp_i} = \frac{4I_{Lf}}{N\pi} \frac{V_{Cp_i}}{\hat{V}_{Cp}} \quad (22b)$$

The model is therefore described by (15) (16) (17) (18) (22)

Small-signal analysis

From the derived phasor-transformed model, a small-signal model can be generated. Equation (15) is modified as follows so that power factor becomes the input:

$$\begin{bmatrix} \dot{I}_{Ls_r} \\ V_{Cs_r} \\ V_{Cp_r} \\ I_{Ls_i} \\ V_{Cs_i} \\ V_{Cp_i} \end{bmatrix} = \begin{bmatrix} 0 & -1 & -1 & \omega_s & 0 & 0 \\ \frac{1}{C_s} & 0 & 0 & 0 & \omega_s & 0 \\ \frac{1}{C_p} & 0 & 0 & 0 & 0 & \omega_s \\ -\omega_s & 0 & 0 & 0 & -1 & -1 \\ 0 & -\omega_s & 0 & \frac{1}{C_s} & 0 & 0 \\ 0 & 0 & -\omega_s & \frac{1}{C_p} & 0 & 0 \end{bmatrix} \begin{bmatrix} I_{Ls_r} \\ V_{Cs_r} \\ V_{Cp_r} \\ I_{Ls_i} \\ V_{Cs_i} \\ V_{Cp_i} \end{bmatrix} + \begin{bmatrix} \frac{2V_i}{\pi L_s} & 0 & 0 \\ 0 & 0 & 0 \\ 0 & -1 & 0 \\ 0 & 0 & 0 \\ 0 & 0 & 0 \\ 0 & 0 & \frac{-1}{C_p} \end{bmatrix} \begin{bmatrix} PF \\ I_{tp_r} \\ I_{tp_i} \end{bmatrix} \quad (23)$$

The equations that describe the phasor-transformed model (16) (17) (18) (22) (23) are linearised about the resonant frequency. Equation (18) can be re-expressed as follows:

$$V_f = \frac{2\sqrt{V_{Cp_r}^2 + V_{Cp_i}^2}}{N\pi} \quad (24)$$

Assuming that variable $X(t)$ can be split into its steady-state and small-signal component as follow:

$$X = X_o + \Delta x \quad (25)$$

where X_o and Δx are the steady-state and small-signal component ,respectively, equation (24) can be written as:

$$V_f = \frac{2\sqrt{(V_{Cp,r,o} + \Delta v_{Cp,r})^2 + (V_{Cp,i,o} + \Delta v_{Cp,i})^2}}{N\pi} \quad (26)$$

Now, linearising (26) about the steady-state components gives:

$$\Delta v_f = \frac{2}{N\pi\sqrt{V_{Cp,r,o}^2 + V_{Cp,i,o}^2}}(V_{Cp,r,o}\Delta v_{Cp,r} + V_{Cp,i,o}\Delta v_{Cp,i}) \quad (27)$$

At resonance, the series inductor current is always sufficient to source the load. Hence, (22) can be written as:

$$I_{p,r} = \frac{4(I_{Lf_o} + \Delta I_{Lf})}{N\pi} \frac{(V_{Cp,r,o} + \Delta v_{Cp,r})}{\sqrt{(V_{Cp,r,o} + \Delta v_{Cp,r})^2 + (V_{Cp,i,o} + \Delta v_{Cp,i})^2}} \quad (28a)$$

$$I_{p,i} = \frac{4(I_{Lf_o} + \Delta I_{Lf})}{N\pi} \frac{(V_{Cp,i,o} + \Delta v_{Cp,i})}{\sqrt{(V_{Cp,r,o} + \Delta v_{Cp,r})^2 + (V_{Cp,i,o} + \Delta v_{Cp,i})^2}} \quad (28b)$$

Equation 28 can be similarly linearised about the steady-state components giving:

$$\Delta i_{p,r} = \frac{4I_{Lf_o}V_{Cp,i,o}^2\Delta v_{Cp,r}}{N\pi(V_{Cp,r,o}^2 + V_{Cp,i,o}^2)^{(3/2)}} - \frac{4I_{Lf_o}V_{Cp,i,o}V_{Cp,r,o}\Delta v_{Cp,i}}{N\pi(V_{Cp,r,o}^2 + V_{Cp,i,o}^2)^{(3/2)}} + \frac{4V_{Cp,r,o}\Delta i_{Lf}}{N\pi\sqrt{V_{Cp,r,o}^2 + V_{Cp,i,o}^2}} \quad (29a)$$

$$\Delta i_{p,i} = \frac{4I_{Lf_o}V_{Cp,r,o}^2\Delta v_{Cp,i}}{N\pi(V_{Cp,r,o}^2 + V_{Cp,i,o}^2)^{(3/2)}} - \frac{4I_{Lf_o}V_{Cp,i,o}V_{Cp,r,o}\Delta v_{Cp,r}}{N\pi(V_{Cp,r,o}^2 + V_{Cp,i,o}^2)^{(3/2)}} + \frac{4V_{Cp,i,o}\Delta i_{Lf}}{N\pi\sqrt{V_{Cp,r,o}^2 + V_{Cp,i,o}^2}} \quad (29b)$$

To form the small-signal model, the steady-state components $V_{Cp,r,o}$, $V_{Cp,i,o}$ and I_{Lf_o} must first be calculated. From (24), the steady-state output filter inductor current is found to be:

$$I_{Lf_o} = \frac{2\sqrt{V_{Cp,r,o}^2 + V_{Cp,i,o}^2}}{N\pi R_L} \quad (30)$$

The transformer primary current components from (22) and (30) are then given by:

$$I_{p,r} = \frac{4I_{Lf}}{N\pi} \frac{V_{Cp,r}}{\sqrt{V_{Cp,r}^2 + V_{Cp,i}^2}} = \frac{8V_{Cp,r}}{N^2\pi^2 R_L} \quad (31a)$$

$$I_{p,i} = \frac{4I_{Lf}}{N\pi} \frac{V_{Cp,i}}{\sqrt{V_{Cp,r}^2 + V_{Cp,i}^2}} = \frac{8V_{Cp,i}}{N^2\pi^2 R_L} \quad (31b)$$

The steady-state conditions are obtained by equating the time derivatives in (23) to zero. Equation (31) is used to replace the I_{tp} components, as follow:

$$\dot{i}_{Ls,r} = 0 = -\frac{1}{L_s}V_{Cs,r} - \frac{1}{L_s}V_{Cp,r} + \omega_s I_{Ls,i} + \frac{2V_i}{\pi L_s} PF \quad (32a)$$

$$\dot{V}_{Cs,r} = 0 = \frac{1}{C_s}I_{Ls,r} + \omega_s V_{Cs,i} \quad (32b)$$

$$\dot{V}_{Cp,r} = 0 = \frac{1}{C_p}I_{Ls,r} + \omega_s V_{Cp,i} - \frac{1}{C_p} \left(\frac{8V_{Cp,r}}{N^2\pi^2 R_L} \right) \quad (32c)$$

$$\dot{i}_{Ls,i} = 0 = -\frac{1}{L_s}V_{Cs,i} - \frac{1}{L_s}V_{Cp,i} - \omega_s I_{Ls,r} \quad (32d)$$

$$\dot{V}_{Cs,i} = 0 = \frac{1}{C_s}I_{Ls,i} - \omega_s V_{Cs,r} \quad (32e)$$

$$\dot{V}_{C_{p_{i0}}} = 0 = \frac{1}{C_p} I_{L_{s_{i0}}} - \omega_s V_{C_{p_{r0}}} - \frac{1}{C_p} \left(\frac{8V_{C_{p_{i0}}}}{N^2 \pi^2 R_L} \right) \quad (32f)$$

As demonstrated earlier, the steady-state power factor does not affect the small-signal analysis hence we shall assume $PF=1$ (resonance), to simplify the analysis. At resonance $I_{L_{s_{i0}}} = 0$ since all the series-inductor current is real. From (32e) this also implies that $V_{C_{s_{r0}}} = 0$. Equation (32a) now allows the calculation of $V_{C_{p_{r0}}}$

$$V_{C_{p_{r0}}} = \frac{2V_i}{\pi} \quad (33)$$

To further simplify the analysis equations derived in [9] concerning the design of LCC current-output resonant converters, based on FMA, can be utilised. It is shown that, at resonance the output voltage of the converter can be expressed as follows:

$$V_o = \frac{V_i G_{tr}}{N} \quad (34)$$

where G_{tr} is the voltage gain of the resonant tank and N is transformer turns ratio when expressed as $N:1$. From this perspective the steady-state output-filter current can be expressed as follow:

$$I_{L_{f_0}} = \frac{V_i G_{tr}}{NR_L} \quad (35)$$

Equating the current in (35) and (30), eliminating $V_{C_{p_{r0}}}$ via use of (33), assuming resonant operation ($PF=1$), and solving for $V_{C_{p_{i0}}}$ gives:

$$V_{C_{p_{i0}}} = -\frac{V_i \sqrt{G_{tr}^2 \pi^4 - 16}}{2\pi} \quad (36)$$

Note that two solutions exist for $V_{C_{p_{i0}}}$ the other having the opposite magnitude. The solution presented in (36) is selected such that the phase of V_{C_p} w.r.t I_{L_s} is negative i.e $\arctan(V_{C_{p_{i0}}} / V_{C_{p_{r0}}}) < 0$.

In [9] it is also shown that for a given converter specification, the resonant tank components can be chosen as follows:

$$C_p = \frac{2\sqrt{G_{tr}^2 \pi^4 - 16}}{\pi^2 N^2 R_L \omega_r} \quad (37a)$$

$$C_s = \frac{2\sqrt{G_{tr}^2 \pi^4 - 16}}{A\pi^2 N^2 R_L \omega_r} \quad (37b)$$

$$L_s = \frac{N^2 R_L ((A+1)G_{tr}^2 \pi^4 - 16)}{2\pi^2 \omega_r G_{tr}^2 \sqrt{G_{tr}^2 \pi^4 - 16}} \quad (37c)$$

where $A=C_p/C_s$, and ω_r is the resonant frequency. These equations will be used to simply the remaining analysis. Substituting (33) and (36), into (32c), and eliminating C_p in (32c) via (37a) gives:

$$I_{L_{s_{r0}}} = \frac{V_i G_{tr}^2 \pi}{N^2 R_L} \quad (38)$$

Eliminating C_s in (32b) via (37b), substituting in (38) and solving for $V_{C_{s_{i0}}}$ then gives:

$$V_{C_{s_{i0}}} = -\frac{AV_i G_{tr}^2 \pi^3}{2\sqrt{G_{tr}^2 \pi^4 - 16}} \quad (39)$$

Since all the steady-state conditions are known (at $PF=1$) the small-signal equations expressed in (27), (29) can be evaluated:

$$\Delta v_f = \frac{2}{N\pi^3 G_{tr}} \left(4\Delta v_{C_p} - \sqrt{G_{tr}^2 \pi^4 - 16} \Delta v_{C_{p_i}} \right) \quad (40)$$

$$\Delta i_{w_r} = \frac{8}{\pi^2 N^2 R_L} \left(1 - \frac{16}{G_{tr}^2 \pi^4} \right) \Delta v_{C_{p_r}} + \frac{32 \sqrt{G_{tr}^2 \pi^4 - 16}}{G_{tr}^2 \pi^6 N^2 R_L} \Delta v_{C_{p_i}} + \frac{16}{G_{tr} \pi^3 N} \Delta i_{L_f} \quad (41a)$$

$$\Delta i_{w_r} = \frac{32 \sqrt{G_{tr}^2 \pi^4 - 16}}{G_{tr}^2 \pi^6 N^2 R_L} \Delta v_{C_{p_r}} + \frac{128}{G_{tr}^2 \pi^6 N^2 R_L} \Delta v_{C_{p_i}} - \frac{4 \sqrt{G_{tr}^2 \pi^4 - 16}}{G_{tr} \pi^3 N} \Delta i_{L_f} \quad (41b)$$

The state-space small-signal model is now formed from (15), (17), (40), (37a) and (41):

$$A = \begin{bmatrix} 0 & -1/L_s & -1/L_s & \omega_r & 0 & 0 & 0 & 0 \\ 1/C_s & 0 & 0 & 0 & \omega_r & 0 & 0 & 0 \\ 1/C_p & 0 & K_{33} & 0 & 0 & (\omega_r + K_{36}) & K_{37} & 0 \\ -\omega_r & 0 & 0 & 0 & -1/L_s & -1/L_s & 0 & 0 \\ 0 & -\omega_r & 0 & 1/C_s & 0 & 0 & 0 & 0 \\ 0 & 0 & (-\omega_r + K_{63}) & 1/C_p & 0 & K_{66} & K_{67} & 0 \\ 0 & 0 & K_{73} & 0 & 0 & K_{76} & 0 & -1/L_f \\ 0 & 0 & 0 & 0 & 0 & 0 & 1/C_f & -1/(C_f R_L) \end{bmatrix} \quad (42)$$

$$B = [2V_{dc}/(\pi L_s) \ 0 \ 0 \ 0 \ 0 \ 0 \ 0 \ 0]$$

$$C = [0 \ 0 \ 0 \ 0 \ 0 \ 0 \ 0 \ 1]$$

$$x = [\Delta I_{L_s} \ \Delta V_{C_{s_r}} \ \Delta V_{C_{p_r}} \ \Delta I_{L_{s_i}} \ \Delta V_{C_{s_i}} \ \Delta V_{C_{p_i}} \ \Delta I_{L_f} \ \Delta V_o]^T$$

$$\begin{aligned} \dot{x} &= Ax + Bu & \text{where } y &= \Delta V_o \\ y &= Cx & u &= \Delta PF \end{aligned}$$

and,

$$\begin{aligned} K_{33} &= -\frac{4\omega_r \sqrt{G_{tr}^2 \pi^4 - 16}}{G_{tr}^2 \pi^4} & K_{36} &= -\frac{16\omega_r}{G_{tr}^2 \pi^4} & K_{37} &= -\frac{8NR_L \omega_r}{G_{tr} \pi \sqrt{G_{tr}^2 \pi^4 - 16}} \\ K_{63} &= -\frac{16\omega_r}{G_{tr}^2 \pi^4} & K_{66} &= -\frac{64\omega_r}{G_{tr}^2 \pi^4 \sqrt{G_{tr}^2 \pi^4 - 16}} & K_{67} &= \frac{2NR_L \omega_r}{G_{tr} \pi} \\ K_{73} &= \frac{8}{L_f G_{tr} \pi^3 N} & K_{76} &= \frac{-2\sqrt{G_{tr}^2 \pi^4 - 16}}{L_f G_{tr} \pi^3 N} \end{aligned}$$

To utilise the model, (42), the converter tank gain and resonant frequency must first be evaluated. These are obtained by solving (37) for A , G_{tr} and ω_r . For instance, to calculate G_{tr} , equate the ω_r term in both (37a) and (37c), and solve for G_{tr} , where $A=C_p/C_s$.

A comparison of the small-signal frequency response prediction between the provided analysis and the prototype system, are given in Fig.3, from which very good agreement is seen to exist. Whilst the state-space description is 8th order, the system is dominantly 3rd order. Moreover, since the small-signal response is found to be constant across the full power-factor range, the small-signal response also provides a good approximation to the large-signal behaviour.

From Fig. 7(a) it can be seen that the 3rd order numerically reduced small-signal model provides an accurate large-signal model. Both the simulated and experimental output voltage closely follows a scaled version of the power factor thus further demonstrating the controller's linear behaviour. From Fig. 7(b) the steady-state linear control behaviour is made evident. As power factor is increased the output voltage across the various loads raises linearly.

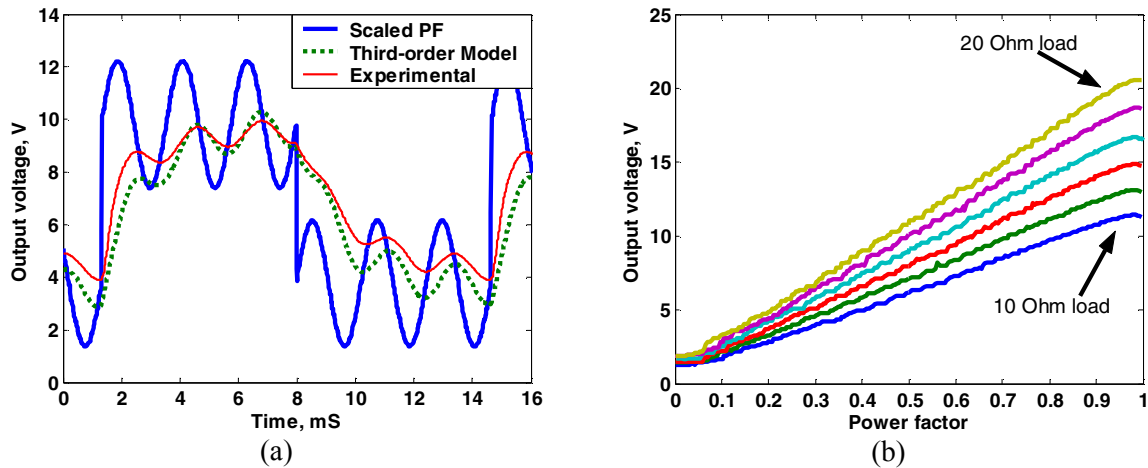


Fig.7 (a) Comparison between experimental and small-signal model response for $R_L=10\Omega$ during a perturbed step change in power factor from PF=0.8 to 0.3. Note that a 3rd order reduced model is utilised for the small-signal response. The power factor is scaled by 12.1V since when the power-factor is unity the theoretical ideal output-voltage of the converter is 12.1V (b) steady-state output voltage as power factor is varied for 10,12,14,16,18,20 Ω loads. Note that 256 linearly spaced power factor points are used for each load.

Conclusion

A control strategy is provided for the LCC current-output resonant converter that is ultimately, more widely applicable to other resonant converter topologies. The methodology is advantageous in that it firstly linearises the steady-state input-to-output conversion ratio and, secondly, the large-signal converter dynamics become predominantly 3rd order. At present, no control methodologies can boast such simple linear behaviour. Through the well-defined behaviour of the power-factor controlled converter, the design of an additional controller to obtain closed-loop output-voltage/current control is greatly simplified, allowing robust and/or well documented adaptive control methods to be applied. This therefore addresses one of the main drawbacks for the use of resonant converters viz. the lack of literature on robust control of such systems.

References

- [1] R. L. Steigerwald, "A comparison of Half-Bridge Resonant Converter Topologies," IEEE Trans. Power Electronics, vol.3, no.2, pp.174-182, April 1988.
- [2] Marian K. Kazimierczuk, Dariusz Czarkowski, Resonant Power Converters, John Wiley sons, inc 1995, ISBN 0-471-04706-6 , Chapter 8 & 17.
- [3] M. Castilla, L. Garcia de Vicuna, J. M. Guerrero, J. Matas, J. Miret, "Sliding-mode control of quantum series-parallel resonant converters via input-output linearization", IEEE Trans. Industrial Electronics, vol.52, no. 2, April 2005, pp.566-575
- [4] A. J. Forsyth, Y. K. E. Ho, "High performance control of the series-parallel resonant converter", IEE Proceedings Electric Power Applications, vol. 144, no. 2, March 1997, pp.131-139
- [5] M. Castilla, L.G. de Vicuna, M. Lopez, V. Barcons, "An Averaged Large-Signal Modelling Method for Resonant Converters", 23rd International Conference on Industrial Electronics, Control and Instrumentation, 1997. IECON 97, vol.2, 9-14 Nov 1997, pp. 444-452.
- [6] Y. Yin, R. Zane. R. Erickson, J. Glaser, "Dynamic analysis of frequency-controlled electronic ballasts," Industry Applications Conference, 2002. 37th IAS Annual Meeting, vol. 1, 13-18 Oct. 2002 pp.685-69.
- [7] Chun. T. Rim, Gyu. H. Cho, "Phasor Transformation and its Application to the DC/AC Analyses of Frequency Phase-Controlled Series Resonant Converters (SRC)," IEEE Trans. Power Electronics, vol.5, no.2, pp.201-211, April 1990.
- [8] S. Ben-Yaakov, S. Glozman, R. Rabinovici, "Envelope Simulation by SPICE-Compatible Models of Electric Circuits Driven by Modulated Signals," IEEE Trans. Industrial Electronics, vol.47, no.1, pp.222-225, February 2000.
- [9] A. J. Gilbert, D. A. Stone, C. M. Bingham, "Rapid design of LCC current-output resonant converters with reduced electrical stresses", 2005 European Conference on Power Electronics and Applications 11-14 Sept. 2005